

Information of the classified information affecting the national defense of the United States within the meaning of the Espionage Act, USC 5051 and 52. Transmission or the revelation of its contents in any manner to an unauthorized person is prohibited by law. Information so classified may be imparted only to persons in the military and naval Services of the United States, appropriate civilian officers and employees of the Federal Government who have a legitimate interest therein, and to United States citizens of known loyalty and character who of necessity must be informed thereof.

RESTRICTED

TECHNICAL NOTES

NATIONAL ADVISORY COMMITTEE FOR AERONAUTICS

No. 797

THE END-PLATE EFFECT OF A HORIZONTAL-TAIL SURFACE
ON A VERTICAL-TAIL SURFACE

By S. Katzoff and William Mutterperl
Langley Memorial Aeronautical Laboratory

Washington
February 1941

NATIONAL ADVISORY COMMITTEE FOR AERONAUTICS

TECHNICAL NOTE NO. 797

THE END-PLATE EFFECT OF A HORIZONTAL-TAIL SURFACE
ON A VERTICAL-TAIL SURFACE

By S. Katzoff and William Mutterperl

SUMMARY

The end-plate effect of the horizontal-tail surface on the vertical-tail surface has been theoretically studied by derivation of the flow corresponding to the condition of minimum induced drag and by solution of the usual lifting-line equations. The results obtained by the two methods were considerably different, indicating that the condition of minimum induced drag (uniform normal induced velocity) is not a close approximation to the actual condition. The derived span load distributions are given, together with equations and curves for the total lift forces and the moments of the horizontal and the vertical-tail surfaces about the intersection. The results obtained indicate a considerable increase in effectiveness of the vertical tail. For example, the effective aspect ratio, in terms of the elliptical airfoil, is about 1.5 times the geometric aspect ratio for a tail group in which the span of the horizontal tail is twice the span of the vertical tail.

INTRODUCTION

The effectiveness of the vertical tail is known to be considerably increased by the presence at its base of the horizontal tail. In conjunction with the tail-surface studies in progress at the NACA, a theoretical study has been made of this end-plate effect for the idealized case of an isolated tail group (fig. 1).

In the usual theoretical end-plate study (references 1 and 2), the problem is simplified by considering only the case of minimum induced drag; that is, the case of constant normal induced velocity along the span of the lifting surface with zero normal induced velocity along the span of the end plate. By this restriction (reference

3), the problem reduces to that of the two-dimensional flow past a figure which represents a cross section of the wake infinitely far downstream; in the present case, the figure is \perp -shaped (fig. 2).

As will be shown, however, the condition of minimum induced drag is physically impossible, for it requires that the end plate have infinite chord. Preliminary studies having indicated that the corresponding inaccuracy might be considerable when the method is applied to the typical tail group, a more general method in which the usual lifting-line equations of the monoplane airfoil were applied was used to obtain a more accurate solution. This method is discussed in part I; the method that assumes minimum induced drag is considered in part II.

SYMBOLS

\perp wake cross section

H, D dimensions of \perp obtained by transformation

h span of vertical tail

d semispan of horizontal tail

r ratio of vertical-tail span to horizontal-tail span
($h/2d$ or $H/2D$)

m a function of $r \left(= \frac{r^2 + 1 - \sqrt{1 + 4r^2}}{r^2} \right)$

S area

c chord

A aspect ratio

l lift per unit length

L total lift or cross-wind force

ρ air density

C_L lift coefficient $\left(\frac{L}{\frac{\rho}{2} V^2 S} \right)$

M moment

α angle of attack

a slope of lift curve $(dC_{Lh}/d\alpha_o)$

a_o slope of section lift curve

V free-stream velocity

w induced velocity

γ circulation per unit length (spanwise) in wake

Γ bound circulation

x, y coordinates of projection of tail group

x_1, y_1 variables of integration

Complex variables:

z plane of \perp (x, y)

ζ plane of unit circle (r, θ)

p auxiliary plane

W potential function (Φ, Ψ)

Subscripts

x point on X axis

y point on Y axis

h vertical tail

d horizontal tail

e effective

o geometric

i induced

I. FINITE HORIZONTAL TAIL

Method

The angle of attack of the vertical-tail surface is assumed to be α_0 and that of the horizontal-tail surface (the end plate) is zero, the corresponding vortex system being as indicated in figure 3. The bound vortex at the base of the vertical tail divides at the intersection and the two halves continue, with opposite rotations, along the horizontal tail.

The normal induced velocity w_x at a point $P(0, y)$ of the horizontal tail (fig. 3) due to the trailing vortex system is, by the Biot-Savart law,

$$w_x(y) = \frac{1}{4\pi} \int_0^h \frac{y}{y^2 + x_1^2} \frac{d\Gamma_h}{dx_1} dx_1 + \frac{1}{4\pi} \int_{-d}^d \frac{1}{y_1 - y} \frac{d\Gamma_d}{dy_1} dy_1 \quad (1)$$

Similarly, for the normal induced velocity w_y at a point $Q(x, 0)$ of the vertical tail,

$$w_y(x) = \frac{1}{4\pi} \int_{-d}^d \frac{x}{x^2 + y_1^2} \frac{d\Gamma_d}{dy_1} dy_1 + \frac{1}{4\pi} \int_0^h \frac{1}{x_1 - x} \frac{d\Gamma_h}{dx_1} dx_1 \quad (2)$$

From the relation between the bound circulation and the effective angle of attack, two additional equations are obtained:

$$\Gamma_d(y) = \frac{a_0 c_d}{2} w_x(y) \quad (3)$$

$$\Gamma_h(x) = \frac{a_0 c_h}{2} [V\alpha_0 + w_y(x)] \quad (4)$$

Derivation of the span load distribution for any given case involves the simultaneous solution of equations (1), (2), (3), and (4). The most practical method found for effecting the solution was a graphical method of successive approximation. A distribution of Γ_d and Γ_h is

assumed and the operations of equations (1) and (2) are performed for a number of values of x and of y to find the normal induced velocities $w_x(y)$ and $w_y(x)$ at these points. Substitution of these values in equations (3) and (4) leads to a span load distribution that, in general, differs from the assumed distribution. The difference between the two distributions will indicate what changes should be made in the assumed distribution to make the corresponding derived distribution agree more closely with it. In the application of this method the process was found to converge very rapidly, so that very little additional computation was required after the first or the second approximation to get accurate agreement.

Results

Span load distributions were calculated for tail groups in which the horizontal and the vertical tails are of elliptical and semielliptical plan form, respectively, and have the same maximum chord. The value of a_0 was assumed to be 5.3 per radian. The results are shown in figure 4 for various aspect ratios and for various ratios of vertical-tail to horizontal-tail span r .

At the intersection of the two tails, the slope of the span load curve is positive for the vertical tail and (negatively) infinite for the horizontal tail. This arrangement can be shown to be the only one consistent with the condition that the bound vortex at the base of the vertical tail divides into two equal parts and continues along the two halves of the horizontal tail with opposite rotations.

The total lift forces on the vertical tails were obtained by integration of the curves of figure 4. From these integrals were derived values of the effective aspect ratio A_e , that is, the actual aspect ratio of an elliptical airfoil having the same lift-curve slope, according to the equation

$$\frac{C_L}{\alpha_0} = a = a_0 \left(1 - \frac{a_0}{a_0 + \pi A_e} \right)$$

The results are summarized in figure 5, where the ratio A_e/A is plotted against r for various values of A . The curve for the condition of minimum induced drag, which is derived in part II, is included in the figure.

The moments of the horizontal and the vertical-tail loads about the point of intersection were also obtained from the span load distributions; they are plotted in figure 6(a). The horizontal-tail moment contributes appreciably toward reducing the resultant moment. The resultant rolling moments about the intersection are given in figure 7(a). For comparison the corresponding moment curves for the minimum induced-drag condition, which are derived in part II, are given in figures 6(b) and 7(b).

II. TAIL SURFACES OF MINIMUM INDUCED DRAG

As stated in the introduction, the case of the tail having minimum induced drag is solved when the two-dimensional flow past a \perp -shaped figure (fig. 2) is determined. The tangential-velocity distribution at such a figure determined the bound vortex system of the tail, which in turn determines the lift distribution.

The Flow Past a \perp -Shaped Figure

Outline of method.— The potential function of the flow past a \perp -shaped figure can be derived from the known potential function of the flow past a unit circle by means of the function that transforms the space around the circle (ξ -plane) to the space around the \perp (z -plane). The transforming function $z = f(\xi)$ must satisfy the following conditions:

- (a) As ξ traces the unit circle, z traces the \perp
- (b) $\lim_{\xi \rightarrow \infty} z = \xi$
- (c) For all points outside the unit circle, the transformation is one to one and conformal.

The function $z = f(\xi)$ can be derived in three steps:

1. By means of a Schwarz-Christoffel transformation (references 4 and 5) the real axis of an auxiliary p -plane is transformed into the \perp , the upper half

of the p-plane going into the region around the \perp
(the z-plane).

2. By the known function

$$\zeta = \frac{p + i}{p - i} \quad (5)$$

the real axis of the p-plane is transformed into the unit circle, the upper half of the p-plane going into the region outside the unit circle (the ζ -plane).

3. The elimination of p from these two functions gives the desired transformation.

Transformation of the p-plane to the z-plane. - By the Schwarz-Christoffel theorem, the real axis of the p-plane is transformed into a \perp by the function whose derivative is

$$\frac{dz}{dp} = K_1 (p - u_1)^{-\frac{\mu_1}{\pi}} (p - u_2)^{-\frac{\mu_2}{\pi}} \dots (p - A)^{-2} (p - \bar{A})^{-2} \quad (6)$$

where μ_1, μ_2, \dots are the exterior angles of the \perp (fig. 8), measured positive counterclockwise; u_1, u_2, \dots are the points on the real axis of the p-plane that transform to the vertices of the \perp ; K_1 is a constant; A is the point in the p-plane that goes into $z = \infty$; and \bar{A} is the conjugate of A . The vertex of the \perp that corresponds to $p = \infty$ is not considered in expression (6). In accordance with equation (5) and condition (b), it is clear that $A = i$. Also, by symmetry, it is permissible to choose $-u_1 = u_4 = a$, $-u_2 = u_3 = b$, and $u_5 = \infty$. Corresponding points in the z- and the p-planes are shown in figures 8 and 9. Equation (6) thus becomes

$$\frac{dz}{dp} = K_1 \frac{p^2 - b^2}{\sqrt{p^2 - a^2} (p^2 + 1)^2} \quad (7)$$

which integrates to

$$z = K_1 B \frac{p\sqrt{p^2 - a^2}}{p^2 + 1} + K_1 C \log \frac{p\sqrt{a^2 + 1} + \sqrt{p^2 - a^2}}{p\sqrt{a^2 + 1} - \sqrt{p^2 - a^2}} + K_2 \quad (8)$$

where

$$B = \frac{1}{2} \frac{1 + b^2}{1 + a^2}$$

$$C = \frac{1}{4} \frac{a^2 - a^2 b^2 - 2b^2}{(1 + a^2)^{3/2}}$$

Equation (8) contains six arbitrary constants; a , b , and the real and the imaginary parts of K_1 and K_2 . These constants are evaluated as follows:

The coefficient C of the logarithm term must be zero in order that z be single valued. By this condition,

$$b^2 = -\frac{a^2}{2 + a^2} \quad (9)$$

The coefficient B now becomes a function only of a :

$$B = \frac{1}{2 + a^2}$$

The point of intersection of the \perp is placed at the origin of the z -plane by putting $z = 0$ for $p = \pm a$. By this condition,

$$K_2 = 0$$

Equation (8) has, at this point, been simplified to the form

$$z = \frac{K_1}{2 + a^2} \frac{p\sqrt{p^2 - a^2}}{p^2 + 1} \quad (10)$$

A substitution for p from equation (5) gives

$$z = \frac{K_1}{4} \frac{\sqrt{1 + a^2}}{2 + a^2} \frac{\xi + 1}{\xi} \sqrt{\xi^2 + 2 \left(\frac{1 - a^2}{1 + a^2} \right) \xi + 1} \quad (11)$$

from which the value of K_1 is determined by the condition that $\lim_{\xi \rightarrow \infty} z = \xi$:

$$K_1 = \frac{4(2 + a^2)}{\sqrt{1 + a^2}}$$

The parameter K_1 is thus real and positive, and the orientation of the \perp is accordingly as shown in figure 10.

A substitution for K_1 in equations (10) and (11) gives

$$z = \frac{4}{\sqrt{1 + a^2}} \frac{p \sqrt{p^2 - a^2}}{p^2 + 1} \quad (12)$$

$$z = \frac{\xi + 1}{\xi} \sqrt{\xi^2 + 2 \left(\frac{1 - a^2}{1 + a^2} \right) \xi + 1} \quad (13)$$

or, with

$$m = \frac{1 - a^2}{1 + a^2}$$

$$z = \frac{\xi + 1}{\xi} \sqrt{\xi^2 + 2m \xi + 1} \quad (14)$$

Finally, m must be determined so that the \perp will have the specified proportions. The length D (corresponding to the semispan of the horizontal tail) is found by substituting $p = b = \frac{a}{\sqrt{2 + a^2}}$ in equation (12).

The length H (corresponding to the span of the vertical tail) is found by substituting $p = \infty$:

$$\left. \begin{aligned} D &= 1 - m & (a) \\ H &= 2\sqrt{2(1 + m)} & (b) \\ r &= \frac{H}{2D} = \frac{\sqrt{2(1 + m)}}{1 - m} & (c) \end{aligned} \right\} \quad (15)$$

From equation (15c), m may be found in terms of r :

$$m = \frac{r^2 + 1 - \sqrt{1 + 4r^2}}{r^2}$$

Thus, as r varies from 0 to ∞ (infinite end plate to no end plate), m varies from -1 to 1. All the parameters of equation (8) have now been determined.

The unit circle $\zeta = e^{i\theta}$ becomes, by equation (14),

$$\begin{aligned} z &= \frac{e^{i\theta} + 1}{e^{i\theta} - 1} \sqrt{e^{i2\theta} + 2m e^{i\theta} + 1} \\ &= 2 \sqrt{2} \cos \frac{\theta}{2} \sqrt{\cos \theta + m} \end{aligned} \quad (16)$$

which relates points on the unit circle to points on the z -plane. Corresponding points of the two figures are shown in figures 10 and 11. The stagnation points of the vertical flow past the circle ($\theta = \pm \frac{\pi}{2}$) transform, by equation (16), to $z = 2 \sqrt{m}$, corresponding to two coincident points on the real axis for $m > 0$ ($r > \sqrt{2}$) and to two symmetrically situated points on the imaginary axis for $m < 0$ ($r < \sqrt{2}$, the more usual case).

The potential function of the flow.— The potential function of the vertically upward flow past the circle with unit velocity is

$$W = \Phi + i \Psi = -i \left(\zeta - \frac{1}{\zeta} \right)$$


For points on the circle

$$\Phi = 2 \sin \theta \quad (17)$$

$$\Psi = 0$$

Equations (16) and (17) suffice to determine the velocity potential on the z -plane.

The Aerodynamic Forces on the Tail Surfaces

Derivation of the span load distribution.— As has been mentioned, the  of figure 2 represents the trailing vortex sheet of a tail group. The potential function just discussed corresponds to the induced flow about the vortex sheet when the induced velocity of the sheet itself is unity. The following calculations will be made for this case of unit induced velocity behind a tail of dimensions H, D ; the final results, however, will be given for any induced velocity w and any tail dimensions h, d .

The circulation per unit length (spanwise) of the trailing vortex sheet at a point $(x, 0)$ is the difference between the velocities on the upper and the lower surfaces at that point, i.e.,

$$\gamma = \left(\frac{\partial \Phi}{\partial x} \right)_1 - \left(\frac{\partial \Phi}{\partial x} \right)_2$$

where the subscripts 1 and 2 refer to the upper and the lower surfaces of the sheet, respectively. The bound circulation Γ at the corresponding point on the vertical tail equals the total circulation in the trailing vortex sheet between this point $(x, 0)$ and the tip $(H, 0)$, i.e.,

$$\Gamma(x) = \int_x^H \gamma \, dx = \int_x^H \left[\left(\frac{\partial \Phi}{\partial x} \right)_1 - \left(\frac{\partial \Phi}{\partial x} \right)_2 \right] dx = \Phi_1 \Big|_x^H - \Phi_2 \Big|_x^H$$

$$\text{or} \quad \Gamma(x) = \Phi_2(x) - \Phi_1(x) \quad (18)$$

$$\text{since} \quad \psi_1(H) = \psi_2(H)$$

The bound circulation at a point $(0, y)$ on the horizontal tail is given by a corresponding expression. Equations (18), (17), and (16) suffice to determine the spanwise distribution of circulation on the vertical tail.

Load distributions have been calculated for various values of r and are given in figures 12 and 13. The curves for the vertical-tail surface have zero slope at $x = 0$, since $x = 0$ ($\cos \theta = -m$) is a stagnation point

of the potential flow where $\left(\frac{\partial \Phi}{\partial x}\right)_1 = \left(\frac{\partial \Phi}{\partial x}\right)_2 = 0$ and, therefore, $\gamma = \frac{d\Gamma}{dx} = 0$.

It will be observed that figures 12 and 13 have non-dimensional coordinates and apply to tails of arbitrary dimensions and arbitrary induced wake velocity.

The total forces.— The total lift forces on the horizontal and the vertical surfaces are proportional to the integrals of Γ across the respective spans. For the vertical tail surface,

$$\begin{aligned} \int_0^H \Gamma(x) dx &= \int_0^H (\Phi_1 - \Phi_2) dx = 2 \int_0^H \Phi_1 dx \\ &= 2 \int_{\theta_1}^{\theta_2} \Phi_1 \frac{dx}{d\theta} d\theta \end{aligned}$$

where $\theta_1 = \cos^{-1}(-m)$, $\theta_2 = 0$, and the integration is along the arc of the unit circle from θ_1 to θ_2 . The velocity potential Φ_1 is given by equation (17) and $\frac{dx}{d\theta}$ ($= \frac{dz}{d\theta}$) is obtained from equation (16).

There results finally

$$\int_0^H \Gamma dx = \pi (1 + m) (3 - m) \quad (19)$$

Similarly, for the integral of Γ on one-half the horizontal tail surface,

$$\begin{aligned} \int_0^D \Gamma dy &= \frac{1}{2} (3 - m) (1 + m) \log \frac{3 - m + 2\sqrt{2(1 - m)}}{1 + m} \\ &\quad - (1 + m) \sqrt{2(1 - m)} \end{aligned} \quad (20)$$

The moment, about the point of intersection, of the lift on the vertical tail is proportional to

$$\int_0^H \Gamma x \, dx = 2 \int_0^H W(z) z \, dz$$

$$= \frac{16}{3} (1 - m^2)^{3/2} + 4(1 + m) \left[\cos^{-1}(-m) + m \sqrt{1 - m^2} \right] \quad (21)$$

Similarly, for the moment of the lift on the horizontal tail,

$$2 \int_0^D \Gamma y \, dy = \frac{16}{3} (1 - m^2)^{3/2} + 4(1 + m) \left[\cos^{-1}(-m) + m \sqrt{1 - m^2} \right]$$

$$- 4\pi(1 + m) \quad (22)$$

In expressions (21) and (22), $\cos^{-1}(-m)$ is taken in the first or the second quadrant. The sum of these expressions corresponds to the resultant moment,

$$\int_0^H \Gamma x \, dx + 2 \int_0^D \Gamma y \, dy =$$

$$\frac{32}{3} (1 - m^2)^{3/2} + 8(1 + m) \left[\cos^{-1}(-m) + m \sqrt{1 - m^2} \right] - 4\pi(1 + m) \quad (23)$$

The foregoing relations hold for the case of unit normal induced velocity and tail dimensions H and D . General formulas, applicable to tails of arbitrary dimensions h and d and arbitrary induced-wake velocity w , are obtained from these relations by multiplying by the proper factors and substituting from equations (15). Thus from equation (19),

$$L_h = \rho V w \left(\frac{h}{H} \right)^2 \pi (1 + m) (3 - m)$$

or

$$L_h = \frac{1}{2} \rho V^2 h^2 \left(\frac{w}{V} \right) \frac{\pi}{4} (3 - m) \quad (a)$$

Similarly,

$$L_d = \frac{1}{2} \rho V^2 \left(\frac{w}{V} \right) d^2 \frac{1+m}{(1-m)^2} \left[(3-m) \log_e \frac{(3-m)+2\sqrt{2(1-m)}}{1+m} - 2\sqrt{2(1-m)} \right] \quad (b)$$

$$M_h = \frac{1}{2} \rho V^2 \left(\frac{w}{V} \right) h^3 \left[\frac{\sqrt{2(1-m)}^{3/2}}{3} + \frac{\pi - \cos^{-1} m + m\sqrt{1-m^2}}{2\sqrt{2}(1+m)} \right] \quad (c)$$

$$M_d = \frac{1}{2} \rho V^2 \left(\frac{w}{V} \right) d^3 \left[\frac{32}{3} \left(\frac{1+m}{1-m} \right)^{3/2} + 8 \frac{1+m}{(1-m)^3} \left(m\sqrt{1-m^2} - \cos^{-1} m \right) \right] \quad (d)$$

$$M = \frac{1}{2} \rho V^2 \left(\frac{w}{V} \right) h^3 \left[\frac{2\sqrt{2}}{3} (1-m)^{3/2} + \frac{m\sqrt{1-m^2} - \cos^{-1} m}{\sqrt{2}(1+m)} \right] \frac{\pi}{2\sqrt{2}(1+m)} \quad (e)$$

$$M = \frac{1}{2} \rho V^2 \left(\frac{w}{V} \right) d^3 \left\{ \frac{64}{3} \left(\frac{1+m}{1-m} \right)^{3/2} + \frac{16(1+m)}{(1-m)^3} \left[m\sqrt{1-m^2} - \cos^{-1} m \right] \frac{8\pi(1+m)}{(1-m)^3} \right\} \quad (f)$$

(24)

The ratio w/V that appears in these expressions will be discussed in the following section.

The limiting forms of these equations for the forces and the moments as the ratio of vertical tail span to horizontal tail span approaches zero or infinity are of interest. Thus, for finite h ,

$$\lim_{r \rightarrow 0} L_h = \frac{1}{2} \rho V^2 h^2 \pi \left(\frac{w}{V} \right)_0$$

$$\lim_{r \rightarrow \infty} L_h = \frac{1}{2} \rho V^2 h^2 \frac{\pi}{2} \left(\frac{w}{V} \right)_\infty$$

$$\lim_{r \rightarrow 0} L_d = \infty$$

$$\lim_{r \rightarrow \infty} L_d = 0$$

$$\lim_{r \rightarrow 0} M_h = \frac{1}{2} \rho V^2 h^3 \frac{4}{3} \left(\frac{w}{V} \right)_0$$

$$\lim_{r \rightarrow \infty} M_h = \frac{1}{2} \rho V^2 h^3 \frac{\pi}{4} \left(\frac{w}{V} \right)_\infty$$

$$\lim_{r \rightarrow 0} M_d = \infty$$

$$\lim_{r \rightarrow \infty} M_d = 0$$

where

$$\left(\frac{w}{V} \right)_0 = \frac{a_0 \alpha_0}{\frac{a_0}{2} + \pi A_0}$$

$$\left(\frac{w}{V} \right)_\infty = \frac{a_0 \alpha_0}{\frac{a_0}{2} + \frac{\pi}{2} A_\infty}$$

In the preceding expressions for w/V , A_0 and A_∞ correspond to semielliptical and elliptical chord distributions, respectively, as will be shown later.

The normal induced velocity and effective aspect ratio.— Inasmuch as $w/2V$ is the induced angle at the vertical-tail surface,

$$C_{L_h} = a_0 \left(\alpha_0 - \frac{w}{2V} \right) \quad (25)$$

Division of equations (24a) by $\frac{1}{2} \rho V^2 S_h$ gives

$$C_{L_h} = \frac{\pi}{4} \frac{wh^2}{VS_h} (3 - m) \quad (26)$$

Eliminating C_{L_h} from equations (25) and (26) gives

$$\frac{w}{V} = \frac{a_0 \alpha_0}{\frac{a_0}{2} + \frac{\pi}{4} \frac{h^2}{S_h} (3 - m)} \quad (27)$$

Substituting for $w/2V$ in equation (25) gives the slope of the lift curve:

$$a \equiv \frac{C_{Lh}}{\alpha_0} = a_0 \left[1 - \frac{a_0}{a_0 + \frac{\pi}{2} \frac{h^2}{S_h} (3 - m)} \right] \quad (28)$$

Now, for a plain elliptical airfoil (reference 6),

$$a = a_0 \left(1 - \frac{a_0}{a_0 + \pi A_e} \right) \quad (29)$$

Comparison of equations (28) and (29) gives a value for the effective aspect ratio of the vertical tail surface:

$$A_e = \frac{h^2}{2S_h} (3 - m)$$

or

$$\frac{A_e}{A} = \frac{3 - m}{2} \quad (30)$$

Values of m and A_e/A have been plotted against r in figure 14. For $r \rightarrow \infty$ (no end plate), $m \rightarrow 1$, the effective aspect ratio is the actual aspect ratio, and the vertical tail-load distribution is elliptical. For $r \rightarrow 0$ (infinite end plate), $m \rightarrow -1$, the effective aspect ratio is twice the actual aspect ratio, and the vertical-tail-load distribution is semielliptical.

Chord distribution.— The chord distribution of the idealized tail-surface combination is related to the derived span load distribution by the equation

$$\Gamma = \frac{cV a_0}{2} (\alpha_0 - \alpha_1)$$

Because both α_0 and α_1 are constant along the span

of the vertical tail, its chord distribution must be proportional to its load distribution. Thus, the curves of figure 12 indicate not only the load but also the chord distributions. It will be seen from the figure that, for values of r lying in the useful working range $r < 1$, the vertical-tail chord distributions approximate closely to the semielliptical. This fact justifies the comparison of results obtained by this method with those of part I (in which the vertical-tail chord distributions were chosen to be semielliptical). For the horizontal tail, both α_0 and α_1 are zero; hence its chord must be infinite.

COMPARISON OF THE TWO METHODS

A comparison of results obtained by the two methods is given in figures 5 and 15. It appears that the implied infinite-chord horizontal tail for the condition of minimum induced drag introduces an excessive end-plate effect. Thus for the tail group of figure 15, the indicated values of C_{L_h} , C_{L_d} , and A_e/A are about 10 percent, 100 percent, and 30 percent higher, respectively, than the values obtained by the lifting-line-equation method.

That the usual method of calculating end-plate effects is considerably in error in the present instance is evident. It may be noted, however, in figure 5, that the relative error decreases with increasing r , that is, with decreasing span of the end plate. The matter is of interest with regard to the theoretical studies of twin tails (references 1 and 2). The relative span of the end plates (the vertical tails in this case) is so small that the error incurred in using the minimum induced-drag method to determine the increased effectiveness of the horizontal tail may well be negligible.

Langley Memorial Aeronautical Laboratory,
National Advisory Committee for Aeronautics,
Langley Field, Va., December 30, 1940.

REFERENCES

1. Hemke, Paul E.: Drag of Wings with End Plates. Rep. No. 267, NACA, 1927.
2. Mangler, W.: The Lift Distribution of Wings with End Plates. T.M. No. 856, NACA, 1938.
3. Munk, Max M.: The Minimum Induced Drag of Aerofoils. Rep. No. 121, NACA, 1921.
4. Mangler, W.: Zwei Bemerkungen zum Abbildungssatz von Schwarz-Christoffel. Z.f.a.M.M., Bd. 18, Heft 4, Aug. 1938, pp. 251-252.
5. Kellogg, Oliver Dimon: Foundations of Potential Theory. Julius Springer (Berlin), 1929, p. 370.
6. Glauert, H.: The Elements of Aerofoil and Airscrew Theory. The Univ. Press (Cambridge), 1930, p. 145.

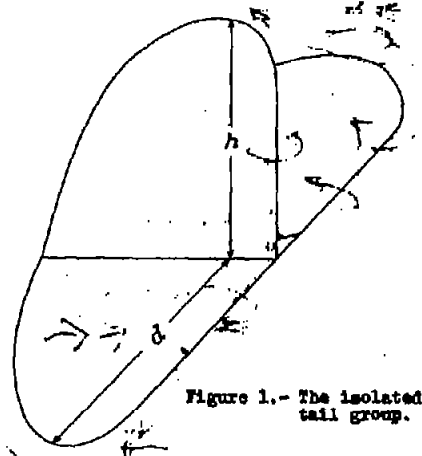


Figure 1.- The isolated tail group.

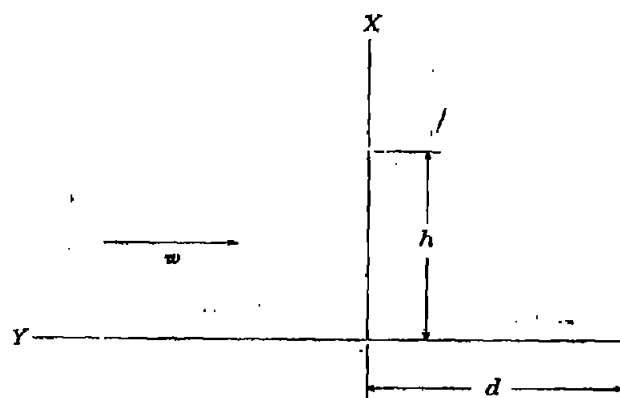


Figure 2.- Cross section of the wake.

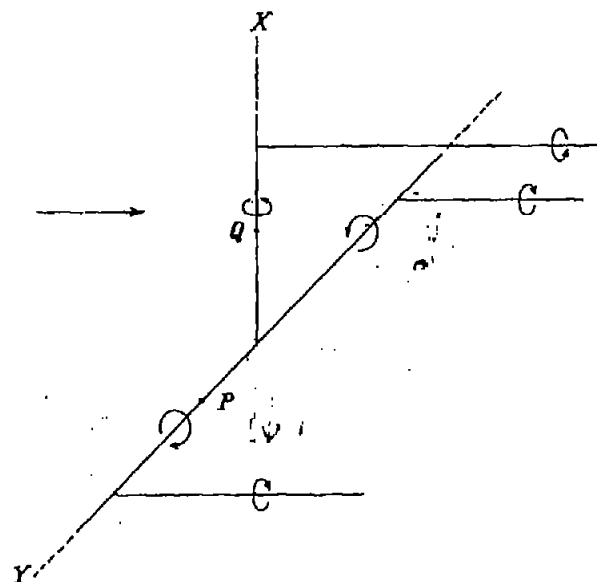
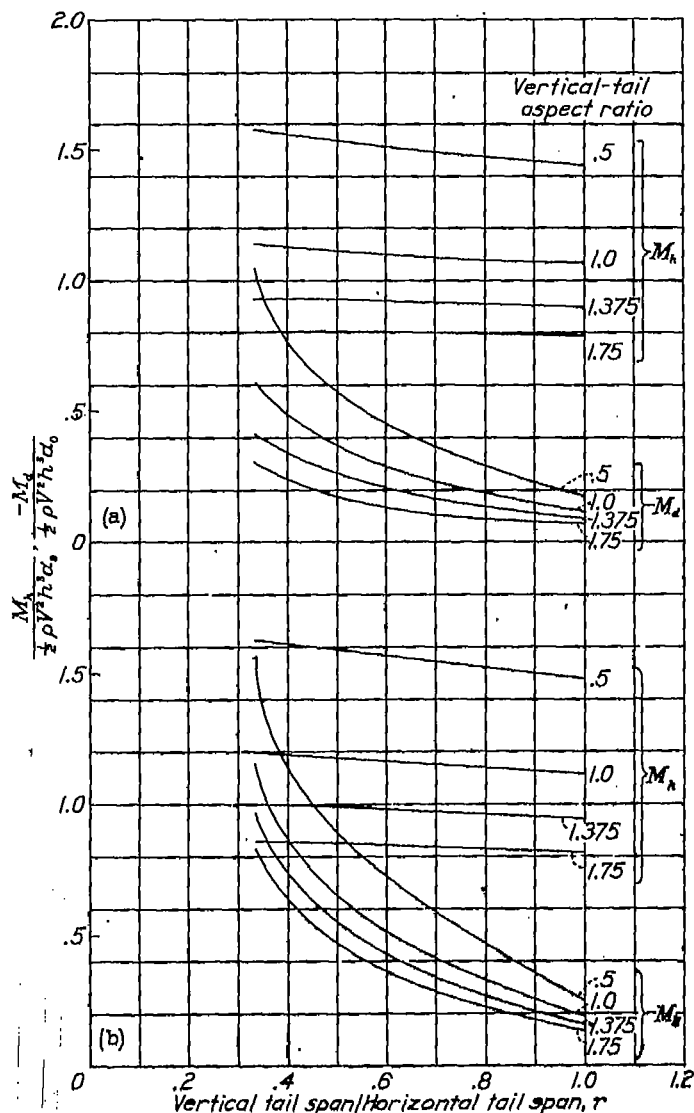
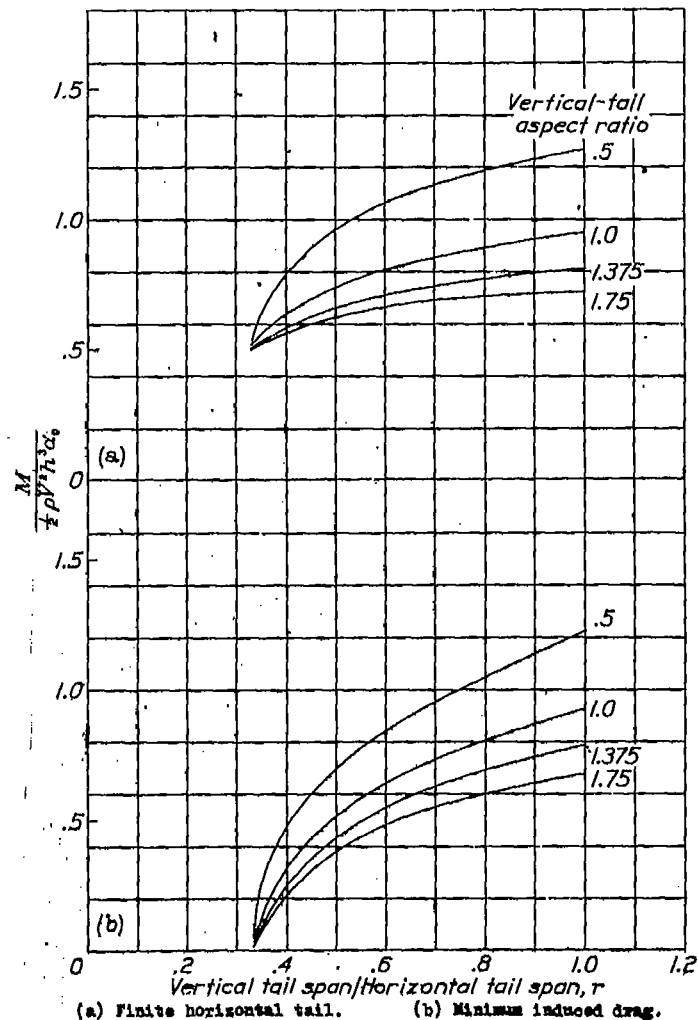


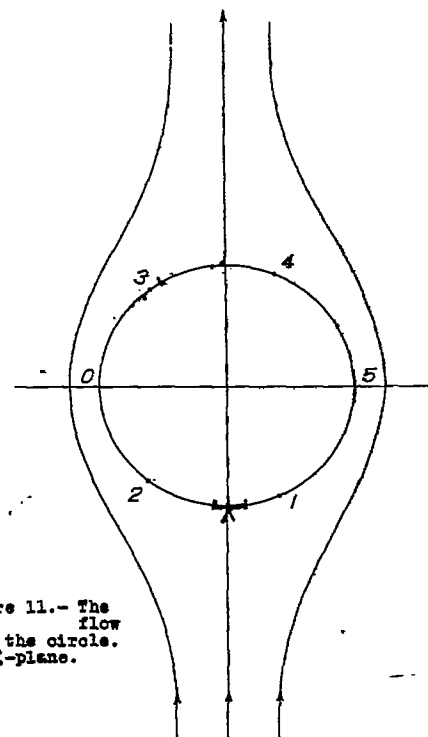
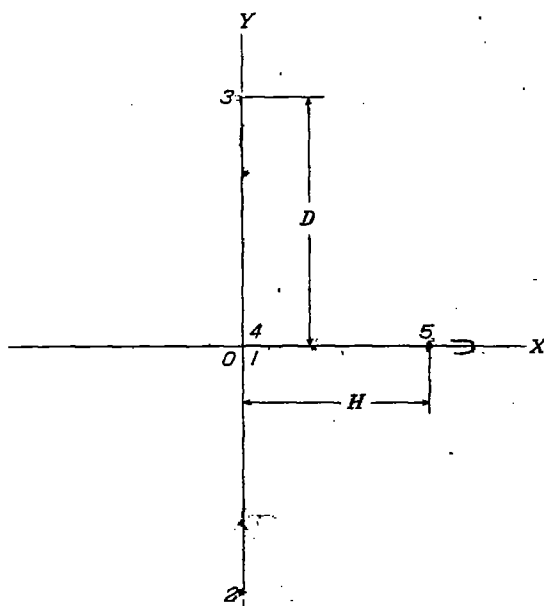
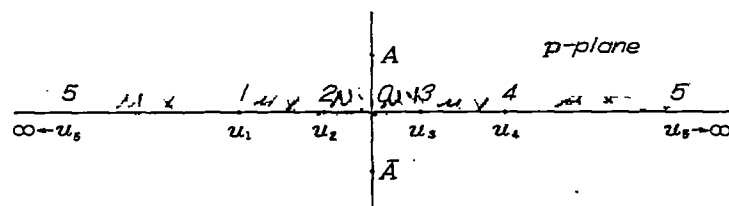
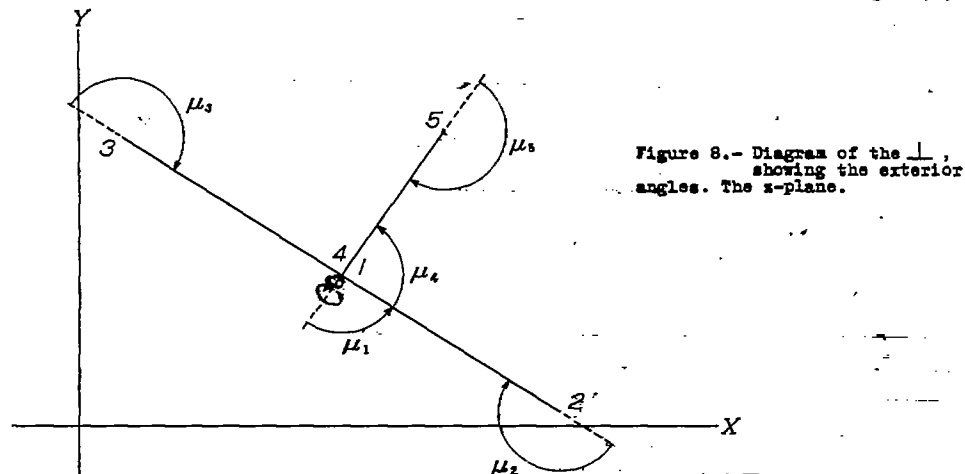
Figure 3.- Representation of the tail vortex system.



(a) Finite horizontal tail. (b) Minimum induced drag.
Figure 6.- The moments of the horizontal and vertical tail forces about the intersection for various vertical-tail aspect ratios.



(a) Finite horizontal tail. (b) Minimum induced drag.
Figure 7.- The resultant moment of the horizontal and vertical tail forces about the intersection for various vertical-tail aspect ratios.



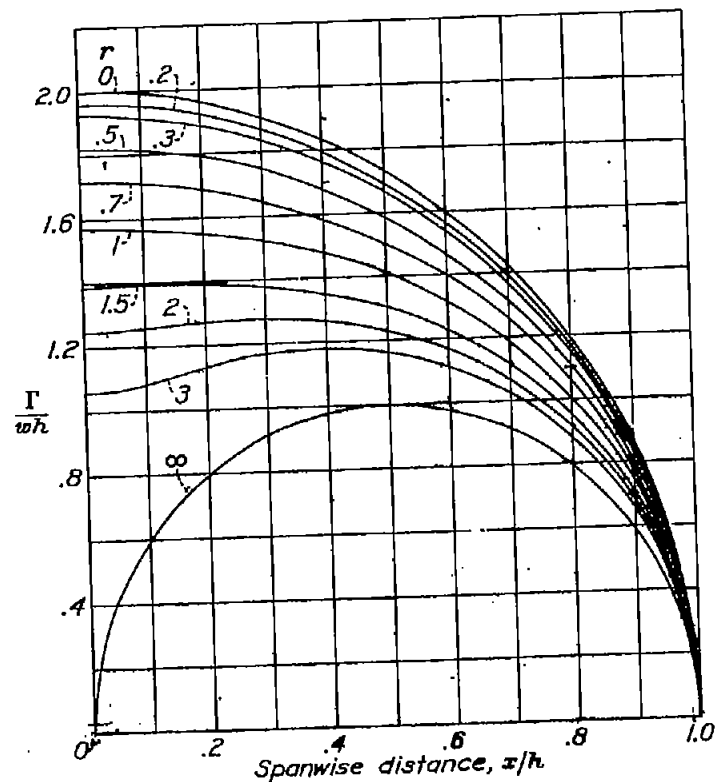


Figure 12.- The span load distribution on the vertical tail surface. Minimum induced drag.

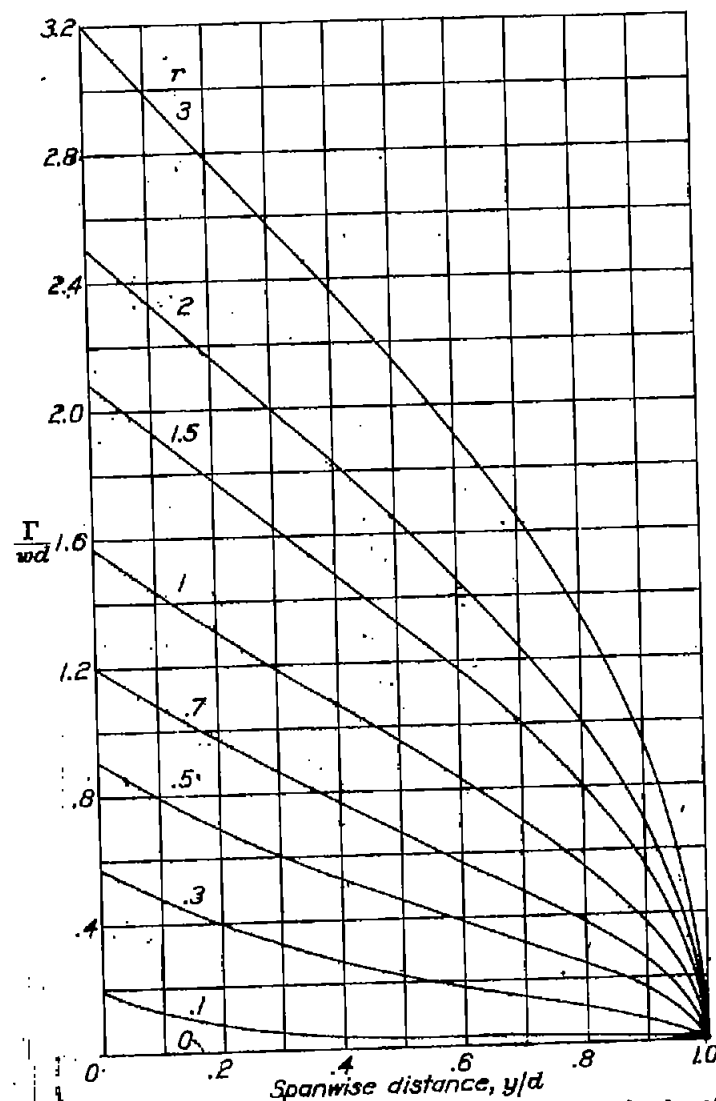


Figure 13.- The span load distribution on the horizontal tail surface. Minimum induced drag.

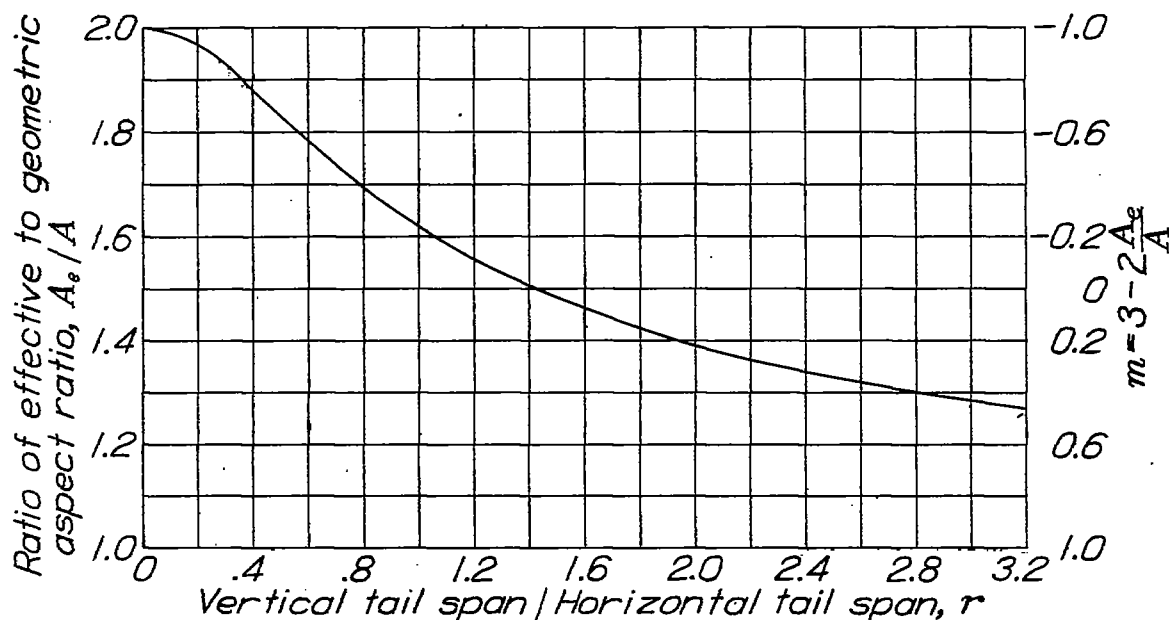


Figure 14.- Variation of A_e/A with r . Minimum induced drag.

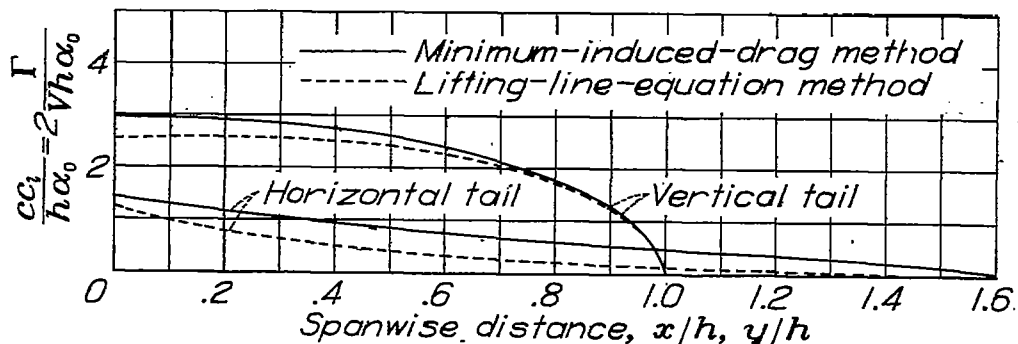


Figure 15.- Comparison of span load distributions calculated by the two methods. Vertical-tail aspect ratio, 1.375 ; r , 0.33.